

# Quasinormal modes of a Generic-class of magnetically charged regular black hole: scalar and electromagnetic perturbations

L. A. López\* and Valeria Ramírez†

*Área Académica de Matemáticas y Física,  
UAEH, Carretera Pachuca-Tulancingo Km. 4.5,  
C P. 42184, Mineral de la Reforma, Hidalgo, México.*

## Abstract

We study the quasinormal modes for scalar and electromagnetic perturbations in a Generic-class of magnetically charged regular black hole that contain the Bardeen-class, Hayward-class, and a New-class solutions. First, the critical values of the charge and mass are obtained. We also described the horizons and the extremal condition of the Generic-class solution. Using the third-order WKB approximation, we can determine the dependence of the quasinormal modes on the parameters of the regular black hole. We have computed the greybody factors and partial absorption cross-section, giving transmission and reflection coefficients of the scattered wave through the effective potentials in the third-order WKB approximation using numerical analysis.

*Keywords: Quasinormal modes, WKB approximation, Black Holes, nonlinear electrodynamics.*

PACS numbers: 04.70.-s, 04.20.Dw, 41.20.Jb, 05.45.-a

---

\*Electronic address: lalopez@uaeh.edu.mx

†Electronic address: ra323273@uaeh.edu.mx

## I. INTRODUCTION

The static and asymptotically flat solutions to the Einstein equations for spherical symmetry that represent Black Holes (HBs) are generally singular at the origin. According to the Penrose conjecture, these singularities must be dressed by an event horizon. The singularities are nonphysical objects so they do not exist in nature. The instabilities leading to the destruction of the event horizon can in principle produce naked singularities, violating the Penrose conjecture.

To avoid the black holes singularity problem, the construction of regular solutions has been proposed. In this sense "regular" means free of curvature divergences. For example, the theory of general relativity coupled to nonlinear electrodynamics is a good candidate. The nonlinear electrodynamics was first considered by Born and Infeld [1], as an attempt to avoid at the classical level the singularity of the electric field of a point charge. In this theory there exists the regular magnetic black hole proposed by Bardeen [2].

Another idea to generate regular solutions is to consider that a regular solution will contain critical scale, mass, and charge parameters restricted by some value that depends only on the type of the curvature invariant, this assumption is called the limiting curvature conjecture [3]. Following the idea of the limiting curvature Hayward [4] proposed a static spherically symmetric black hole that near the origin behaves like a de Sitter spacetime, its curvature invariants being everywhere finite and satisfying the weak energy condition.

A Generic-class that contains the solutions of Bardeen, Hayward and other is addressed in [5] where the authors presented a procedure for constructing regular solutions of charged black holes in general relativity coupled to nonlinear electrodynamics (NLED).

A BH always interacts with matter and fields around, and as a result of these interactions, it takes on a perturbed state regardless of whether it is regular or not then when a BH is perturbed, the resulting behavior can be described in a corresponding stage as damped oscillations with complex frequencies, the modes of such oscillations are called quasinormal modes (QNM).

The frequencies of QNM of a BH are complex quantities that corresponds to solutions of the perturbed equations, which satisfy the boundary conditions of the purely ongoing wave at the horizon and the purely outgoing wave at infinity. In addition, its real part describes the real oscillation frequency and the imaginary part describes the damping of

these oscillations. The importance of quasinormal modes lies in the analysis of the stability of BHs, however, they also play another fundamental role in characterizing gravitational wave signals as the ones recently detected by LIGO and VIRGO [6]. The literature proposes several numerical methods to calculate the QNM for example, the continued fraction method [7], finite difference method [8] and WKB [9] approximation method, this being latter the most used.

Different investigations have emerged about QNM for a variety of scenarios in (NLED). For example; QNM of Bardeen BH [10], QNM of charged BHs in Einstein–Born–Infeld gravity [11] and Bronnikov BH [12]. In [13] and [14] where they have considered; scalar, electromagnetic and gravitational perturbations. The QNM of Hayward, Bardeen, and Ayón–Beato–García regular black holes are compared in [15]. Also, in [16], the behavior of QNM is shown to apply the Eikonal regime and effective geometry. The study of the quasinormal modes (QNM) in the eikonal approximation of the Einstein–Euler–Heisenberg BH is aborded in [17].

The paper is organized as follows: In the next Section a short summary of the Generic–class of magnetically charged regular BH is presented. In Section III, we derive the effective potentials that arise in the scalar and electromagnetic perturbations and we present the behavior of the potentials for the Bardeen–class, Hayward–class and a New–class solutions. In Section IV we present the QNM of the scalar and electromagnetic perturbations, we compare them with the corresponding different values of the constant that characterizes the strength of nonlinearity of the electromagnetic field. The reflection and transmission coefficients are studied considering the different perturbations in Sec. V. Conclusions are given in Section VI.

## II. REGULAR BLACK HOLES WITH MAGNETIC CHARGES

The action for gravitation coupled to a non–linear electrodynamics [18] is;

$$S = \frac{1}{16\pi} \int d^4x \sqrt{-g} [R - \mathcal{L}(F, G)], \quad (1)$$

where  $R$  is the scalar curvature.  $\mathcal{L}$  is an arbitrary function of the electromagnetic invariants  $F = F_{\beta\lambda}F^{\beta\lambda}$  and  $G = F_{\beta\lambda}\mathcal{F}^{\beta\lambda}$ , where  $F_{\beta\lambda} = \partial_\beta A_\lambda - \partial_\lambda A_\beta$  being the electromagnetic field tensor and  $\mathcal{F}^{\beta\lambda}$  is the dual field electromagnetic tensor. In this work we restrict ourselves

to Lagrangians  $\mathcal{L}$  that only depend on  $F$ . The energy momentum tensor is;

$$T_{\beta\lambda} = 2(\mathcal{L}_F F_\beta^\gamma F_{\lambda\gamma} - \frac{1}{4}g_{\beta\lambda}\mathcal{L}), \quad (2)$$

the subindex  $F$  represents the derivative with respect to  $F$ .

If we consider the spherical coordinates  $x^\mu = (t, r, \theta, \phi)$  and for a static spherically symmetric background;

$$ds^2 = -f(r)dt^2 + \frac{1}{f(r)}dr^2 + r^2d\Omega^2, \quad (3)$$

with  $f(r) = 1 - m(r)/r$ , considering a mass distribution function  $m(r)$  positively finite. To exclude the space-time singularity at the origin, we consider the smooth function  $m(r)$  that is at least three times differentiable and approaches zero sufficiently fast in the limit  $r \rightarrow 0$ , the third order derivative is finite and it presents some low-lying curvature polynomials (see [5]).

The line element (3) satisfies the symmetry  $T_t^t = T_r^r$  and the general 4-potential can be written in the form;

$$A_\beta = \varphi(r)\delta_\beta^t - q \cos\theta\delta_\beta^\phi \quad (4)$$

Where  $\varphi(r)$  is the electric potential and  $q$  is the magnetic charge.

The Generic-class of magnetically charged regular BH (see [5]) is given by the metric function ;

$$f(r) = 1 - \frac{2Mr^{\mu-1}}{(r^\mu + q^\nu)^{\mu/\nu}} \quad (5)$$

Where  $M$  is the gravitational mass,  $\mu \geq 3$  is a dimensionless constant that characterizes the strength of nonlinearity of the electromagnetic field and  $\nu > 0$  is also a dimensionless constant. The form of  $f(r)$  in (5) corresponding to the Lagrangian density is given by;

$$\mathcal{L} = \frac{4\mu}{\alpha} \frac{(\alpha F)^{\frac{\nu+3}{4}}}{[1 + (\alpha F)^{\frac{\nu}{4}}]^{1+\frac{\mu}{\nu}}}. \quad (6)$$

$\alpha > 0$  has the dimension of length squared and it is related to the gravitational mass of the form  $M = \alpha^{-1}q^3$ . Also, the construction of charged BHs has been studied in [19] [20].

We can obtain several classes of regular BHs such as Bardeen-class solutions ( $\nu = 2$ ), Hayward-class solutions ( $\nu = \mu$ ) and a New-class ( $\nu = 1$ ). The solution (5) represents BH

with one or two horizons it can also represent extremal BH with one horizon, the number of horizons depends entirely on the choice of the values of parameters  $\mu$ ,  $\nu$ ,  $M$  and  $q$ .

The event horizons ( $r_h$ ) of the space–time (3) are defined by the divergence of the metric function  $g_{rr}$ , this corresponds to the positive roots of the metric function  $f(r)$  in (5), for this analysis we express radial distance and the parameter  $q$  in units of mass as  $r \rightarrow r/M$ ,  $q \rightarrow q/M$ .

Now we determine the range of values of  $q$ , so that the different line elements represent a black hole or an extremal black hole, for this, we make use of the method described in [21, 22]. First when we consider  $f(r_h) = 0$  in (5) the  $q^\nu$  parameter can be parametrized as a function of  $r_h$  as;

$$q^\nu(r_h) = -r_h^\nu + \frac{2^{\nu/\mu}}{(r_h^{1-\mu})^{\nu/\mu}} \quad (7)$$

where  $q^\nu(r_h)$  has extremes  $\left(\frac{dq^\nu(r_h)}{dr_h} = 0\right)$  in certain  $r_h = r_{crit}$ , given by;

$$r_{crit} = \left(\frac{2^{\nu/\mu}(\mu-1)}{\mu}\right)^{\mu/\nu} \quad (8)$$

Then the critical value of the parameter  $q^\nu$  is given in terms of  $\mu$  as;

$$q_{crit}^\nu = q^\nu(r_{crit}) = \frac{\mu \left(\frac{(\mu-1)2^{\nu/\mu}}{\mu}\right)^{\mu/\nu}}{\mu-1} - \left(\frac{(\mu-1)2^{\nu/\mu}}{\mu}\right)^\mu, \quad (9)$$

so the magnetically charged regular BH (5) has one ( $r_+$ ) or two ( $r_{in}$  and  $r_{out}$ ) horizons for values of  $q^\nu \leq q_{crit}^\nu$ .

The extreme cases (when the inner and outer horizons merge into a single horizon  $r_+$ ) can be obtained when the conditions  $f(r) = 0$  and  $\frac{d}{dr}f(r) = 0$  are satisfied simultaneously. Introducing the  $q^\nu$  of (7) in  $\frac{d}{dr}f(r) = 0$ , we obtain one real root denoted by  $r_+ = r_{crit}$ .

In Fig. 1 a) the behavior of  $q_{crit}^\nu$  as function of  $\mu$  is shown. The lines  $q_{crit}^\nu$  contain the values of  $(q^\nu, \mu)$  where the magnetically charged regular black holes have one horizon, while in the regions below the lines, there are two horizons and there are no horizons obtained in the regions above the lines.

Thus, the ranges of the charge parameter increase as  $\mu$  increases in the Hayward–class solutions ( $\nu = \mu$ ) and decrease as  $\mu$  increases in the Bardeen–class ( $\nu = 2$ ) and in the New–class ( $\nu = 1$ ). It is also possible to mention that the range  $[q]_{\nu=\mu} > [q]_{\nu=2} > [q]_{\nu=1}$ . In [23]

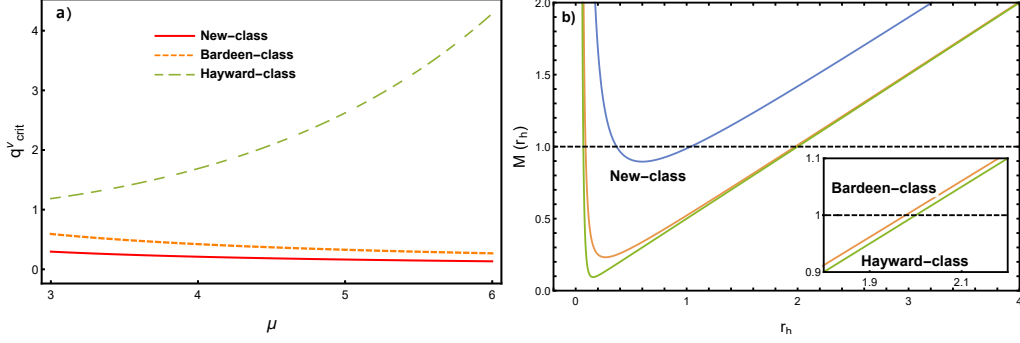


FIG. 1: The figure a) shows the behavior of  $q_{crit}^\nu$  in function of  $\mu$ . Notice that as  $\mu$  grows,  $q_{crit}^\nu$  also grows only in the case of Hayward-class. In the figure b) the behavior of  $M$  in function of  $r_h$  is shown with  $\mu = 6$  and  $q = 0.12$

the ranges of  $q$  for the magnetically charged regular black holes with  $\mu = 3$  were studied.

We complement the analysis of the horizons of Generic-class, studying the behavior of  $M(r_h, q)$  in (5).

$$M(r_h, q) = \frac{1}{2} r_h^{1-\mu} (q^\nu + r_h^\nu)^{\mu/\nu} \quad (10)$$

Note that as  $\mu \geq \nu$  the function  $M(r_h, q) \rightarrow \infty$  for  $r_h \rightarrow \infty$ . A critical mass  $M_*$  exists (see equation (11)) and a radius  $r_* = q(-1 + \mu)^{1/\nu}$  such that Generic-class does not have a horizon if  $M < M_*$ , in the case of  $M_* = M$  it has one horizon at  $r = r_*$  and if  $M_* < M$  it has two horizons.

$$M_* = \frac{1}{2} q \mu^{\mu/\nu} (\mu - 1)^{\frac{1-\mu}{\nu}} \quad (11)$$

In Fig.1 b) the behavior of  $M$  as function of  $r_h$  is shown for  $\mu = 6$ , it can be seen that  $M_{*(Hayward-class)} < M_{*(Bardeen-class)} < M_{*(New-class)}$ . From the Fig. 1 b) we can conclude that when we fix a value of  $M$ , for example  $M = 1$  as in Fig.1 b) is shown, the  $r_{out}$  horizon of Hayward-class is larger compared with  $r_{out}$  horizons of Bardeen-class and New-class.

### III. SCALAR AND ELECTROMAGNETIC PERTURBATIONS

The general perturbation equation for the massless scalar field in the curved space–time is given by the Klein–Gordon equation

$$\frac{1}{\sqrt{-g}}\partial_{\mu}(\sqrt{-g}g^{\mu\nu}\partial_{\nu})\Phi = 0. \quad (12)$$

Substituting Eq. (3) into Eq. (12), and using the ansatz for the scalar field  $\Phi$  we have

$$\Phi = e^{-i\omega t}Y_l^m(\theta, \phi)\frac{\xi(r)}{r}. \quad (13)$$

After introducing the tortoise coordinates change

$$dr_* = \frac{dr}{f(r)}, \quad (14)$$

we obtain the radial perturbation equation

$$\frac{d^2\xi(r)}{dr_*^2} + [\omega^2 - V(r)]\xi(r) = 0, \quad (15)$$

where the generalized form of the effective potential for scalar and electromagnetic test fields, can be written as

$$V(r) = f(r) \left[ \frac{l(l+1)}{r^2} + (1-s) \left( \frac{f'(r)}{r} \right) \right], \quad (16)$$

Here,  $l$  is the spherical harmonic index and it is restricted by  $l \geq s$ , and  $s = 0, 1$  denotes the spin of the perturbation: scalar and electromagnetic (see [24, 25]). We can see from Eq. (16) that the effective potential  $V$  depends on the parameter of the function  $f(r)$  and harmonic index  $l$ .

The effective potential  $V(r)$  has asymptotic value  $V(r) \approx 0$  when  $r \rightarrow \infty$ , in both cases, scalar and electromagnetic perturbation.

We plot the effective potentials for the scalar and electromagnetic perturbations. The Fig 2 a), Fig 2 b) and Fig 2 c) show the dependence of effective potentials (16) with the parameter  $\mu$  for New–class, Bardeen–class and Hayward–class respectively. We notice that in the case of New–class and Bardeen–class the potentials increase as  $\mu$  increases. When  $\mu$  is increased, the maximum of potentials increase and their position moves toward the left for both perturbations, this implies that the strength of nonlinearity of the electromagnetic field increases the magnitudes of the different potentials. But in the case of Hayward–class,

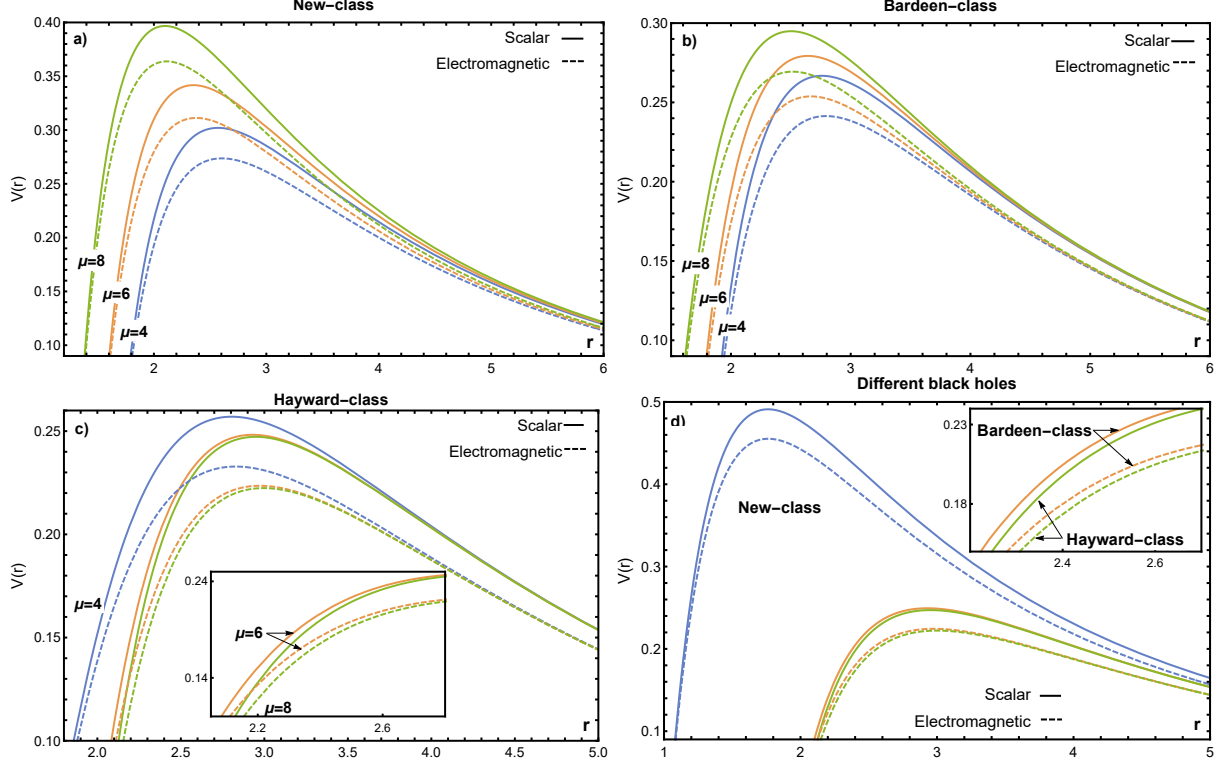


FIG. 2: a) The behavior of the effective potential for the New-class is shown for various values of  $\mu$ , with  $M = 1$ ,  $l = 2$  and  $q = 0.07$ . b) The behavior of the effective potential for the Bardeen-class is shown for various values of  $\mu$ , with  $M = 1$ ,  $l = 2$  and  $q = 0.41$ . c) The behavior of the effective potential for the Hayward-class is shown for various values of  $\mu$ , with  $M = 1$ ,  $l = 2$  and  $q = 1.13$ . d) The behavior of the effective potential for the different BH is compared with  $\mu = 6$ ,  $M = 1$ ,  $l = 2$  and  $q = 0.12$ . In all figures, the effective potential of the scalar perturbation is denoted with a solid line and the electromagnetic perturbation is denoted with a dashed line.

when  $\mu$  increases, the maximum of potentials decrease and its position moves toward the right. We can also mention that in all the cases  $V(r)_{elec} < V(r)_{sc}$ .

On the other hand, in Fig. 2 d) the different effective potentials of the three BHs are compared with the same charge. We can observe that  $V(r)_{Hayward-class} < V(r)_{Bardeen-class} < V(r)_{New-class}$  in both perturbations, we note that the scalar and electromagnetic perturbations of the New-class are higher than the scalar and electromagnetic perturbations of the Hayward-class and Bardeen-class.

Bardeen-class and Hayward-class potentials are very close to each other, the difference is shown in the small box.



In general, the behavior for electromagnetic and scalar perturbation is similar. However, the height of the maximum potential is much higher for scalar perturbations, and the maximum of the potential depends on  $\mu$ . It is also possible to mention that the maximum height of the potentials increases as  $l$  increases with a  $\mu$  fixed.

#### IV. QUASINORMAL MODES OF BLACK HOLES

For a BH, the QNM correspond to solutions of the wave equation given in Eq. (15), which satisfy the appropriate boundary conditions. At the horizon, the boundary condition is such that the wave has to be purely ingoing  $\xi(r) \sim e^{-i\omega r^*}$  and purely outgoing at spatial infinity  $\xi(r) \sim e^{i\omega r^*}$ , that wave function  $\Phi$  has a time dependency  $\Phi(t, r, \phi, \theta) \sim e^{-i\omega t}$ . Only a discrete set of complex frequencies satisfies these conditions, that are  $\omega = \omega_r + i\omega_i$ .

The real part of the frequency,  $\omega_r$  represents the real oscillation of the black hole, which is always positive. On the other hand, the imaginary part of the frequency  $\omega_i$  can be positive or negative. In the case where  $\omega_i < 0$ , we have a damped oscillation, because  $\Phi$  decreases as time progresses and eventually tends to zero for very long periods of time, for which gradually the oscillation of the black hole will cease (stable solution).

In the literature several methods are proposed to calculate the quasi-normal modes, the WKB method is one of the most used. Using the code provided in [26], in the tables I and II we show the calculated frequencies with different orders of WKB and different values of  $\mu$ .

In Table I, the spectrum for the  $\omega_r$  frequencies of the QNM of the scalar and electromagnetic perturbations is shown up to the sixth order. We can observe that in all orders, the  $\omega_{r_{sc}}$  and  $\omega_{r_{elec}}$  of the New-class are more significant than the frequencies of Bardeen-class and Hayward-class. On the other hand, the values of  $\omega_r$  of Bardeen-class are very close to the values of  $\omega_r$  of Hayward-class for both perturbations.

The  $|\omega_i|$  frequencies of the QNM of the scalar and electromagnetic perturbations are shown in the Table II, we can observe that in all orders the values of  $|\omega_i|$  are very close for the three-class black holes and in general  $|\omega_{i_{sc}}| > |\omega_{i_{elec}}|$ .

To evaluate the QNM, we use the third-order WKB approximation method developed by Schutz, Will [9] and Iyer [27]. The formula for the quasi-normal frequencies is:

$\mu$	q	WKB order	Scalar			Electromagnetic		
			New-class	Bardeen-class	Hayward-class	New-class	Bardeen-class	Hayward-class
4	0.17	1	0.729515	0.563434	0.561097	0.703442	0.537951	0.535532
		2	0.656427	0.475397	0.471966	0.629307	0.449102	0.445595
		3	0.652737	0.466936	0.463196	0.625257	0.439689	0.435833
		4	0.653249	0.467554	0.463759	0.625848	0.440358	0.436435
		5	0.653299	0.467683	0.463866	0.625916	0.440495	0.436541
		6	0.653298	0.467647	0.463853	0.625903	0.440464	0.436542
6	0.12	1	0.751093	0.562837	0.561096	0.725453	0.537333	0.535531
		2	0.682926	0.474519	0.471961	0.656535	0.448203	0.445589
		3	0.679575	0.46598	0.463192	0.652914	0.438702	0.435828
		4	0.680296	0.466583	0.463753	0.653722	0.439353	0.436428
		5	0.680348	0.466706	0.463859	0.653791	0.439483	0.436533
		6	0.680345	0.466677	0.463847	0.653776	0.43946	0.436534
8	0.07	1	0.687894	0.561882	0.561096	0.661698	0.536344	0.535531
		2	0.609731	0.473113	0.471961	0.582411	0.446766	0.445589
		3	0.605126	0.464448	0.463192	0.577315	0.437123	0.435828
		4	0.605639	0.465028	0.463753	0.577918	0.437745	0.436428
		5	0.605711	0.465142	0.463859	0.578015	0.437862	0.436533
		6	0.605696	0.465122	0.463847	0.577981	0.437852	0.436534

TABLE I: Quasi-normal frequencies  $\omega_r$  for scalar and electromagnetic perturbation for different order WKB and different values of  $\mu$ ,  $l = 2$ ,  $n = 0$  and  $M = 1$ .

$\mu$	q	WKB order	Scalar			Electromagnetic		
			New-class	Bardeen-class	Hayward-class	New-class	Bardeen-class	Hayward-class
4	0.17	1	0.277043	0.259483	0.260209	0.273083	0.253476	0.254101
		2	0.307889	0.307535	0.309349	0.305254	0.303623	0.305387
		3	0.299943	0.294286	0.295797	0.296814	0.289519	0.290958
		4	0.299708	0.293898	0.295438	0.296534	0.289079	0.290557
		5	0.299817	0.294103	0.295606	0.296678	0.289289	0.290715
		6	0.299818	0.294125	0.295614	0.296684	0.289309	0.290715
6	0.12	1	0.270338	0.259675	0.260216	0.266525	0.253643	0.254108
		2	0.297321	0.308007	0.309361	0.294503	0.304083	0.305399
		3	0.289541	0.294682	0.29581	0.286339	0.289896	0.290972
		4	0.289235	0.294301	0.295452	0.285984	0.289467	0.290571
		5	0.289357	0.294496	0.295619	0.286141	0.289663	0.290729
		6	0.289358	0.294515	0.295627	0.286147	0.289678	0.290728
8	0.07	1	0.27655	0.259977	0.260216	0.272104	0.253903	0.254108
		2	0.312002	0.308756	0.309361	0.309147	0.304812	0.305399
		3	0.302904	0.295303	0.29581	0.299436	0.290493	0.290972
		4	0.302647	0.29494	0.295452	0.299124	0.29008	0.290571
		5	0.30279	0.29512	0.295619	0.299311	0.290255	0.290729
		6	0.302798	0.295133	0.295627	0.299329	0.290262	0.290728

TABLE II: Quasi-normal frequencies  $|\omega_i|$  for scalar and electromagnetic perturbation for different order WKB and different values of  $\mu$ ,  $l = 2$ ,  $n = 0$  and  $M = 1$ .

$$\omega^2 = \left[ V_0 + (-2V_0'')^{1/2} \Lambda(\alpha) \right] - i\alpha (-2V_0'')^{1/2} [1 + \Omega(\alpha)] , \quad (17)$$

where

$$\begin{aligned}\Lambda(\alpha) &= \frac{1}{(-2V_0'')^{1/2}} \left\{ \frac{1}{8} \left( \frac{V_0^{(4)}}{V_0''} \right) \left( \frac{1}{4} + \alpha^2 \right) - \frac{1}{288} \left( \frac{V_0'''}{V_0''} \right)^2 (7 + 60\alpha^2) \right\}, \\ \Omega(\alpha) &= \frac{1}{-2V_0''} \left\{ \frac{5}{6912} \left( \frac{V_0'''}{V_0''} \right)^4 (77 + 188\alpha^2) - \frac{1}{384} \left( \frac{V_0'''}{V_0''} \right)^2 \left( \frac{V_0^{(4)}}{V_0''} \right) (51 + 100\alpha^2) \right. \\ &\quad \left. - \frac{1}{288} \left( \frac{V_0^{(6)}}{V_0''} \right) (5 + 4\alpha^2) + \frac{1}{288} \left( \frac{V_0'''}{V_0''} \right)^2 \left( \frac{V_0^{(5)}}{V_0''} \right) (19 + 28\alpha^2) + \frac{1}{2304} \left( \frac{V_0^{(4)}}{V_0''} \right)^2 (67 + 68\alpha^2) \right\},\end{aligned}\tag{18}$$

with

$$\alpha = n + \frac{1}{2}, \quad V_0^{(n)} = \left. \frac{d^n V(r)}{dr_*^n} \right|_{r_* = r_*(r_p)},\tag{20}$$

where  $r_*(r_p)$  indicates the value of the variable  $r_*$  at which the effective potential ( $V(r)$ ) obtains its maximum ( $V_0$ ).

In Tables III–IV we show the spectrum for the frequencies ( $\omega_r$  and  $|\omega_i|$ ) of the QNM of the scalar and electromagnetic perturbations for different values of  $n$ ,  $l$  and  $q$ , we use the third–order WKB approximation method. It is worth mentioning that WKB method works best for  $l > n$ , while for  $l = n$ , it does not provide satisfactory results, as other authors have shown (see [28]). It is possible to observe that for  $n$ , and  $q$  fixed, the imaginary and real parts of the QNM increase as  $l$  augments; it occurs in all cases of the different black holes.

The real part of the quasi–normal frequencies as a function of  $q$  is shown in Fig. (3) for the scalar and electromagnetic perturbations. The Fig 3 a), Fig 3 b) and Fig 3 c) show the dependence of  $\omega_r$  (17) with the parameter  $\mu$  for New–class, Bardeen–class and Hayward–class respectively. We can see that to both perturbations the real value of the QNM frequency  $\omega_r$  increases when  $q$  increases, in the cases of New–class (Fig. 3 a) ) and Bardeen–class (Fig. 3 b)), this means the perturbation in the fundamental mode ( $n = 0$ ) with larger  $q$  leads to a more intense QNM oscillation. It is also possible to mention that  $\omega_{r_{sc}} > \omega_{r_{elec}}$ . Now, in both perturbations if  $\mu$  increases,  $\omega_r$  increases but the range of values for  $q$  decreases i.e., the strength of nonlinearity of the electromagnetic field increases the magnitudes of oscillation and decreases the allowed  $q$  values.

In the Hayward–class we observe (see Fig 3 c) )that  $\omega_r$  increases if  $\mu$  decreases and  $\omega_{r_{sc}} > \omega_{r_{elec}}$ , in the case  $\nu = 8$ ,  $\omega_r$  decreases when  $q$  increases, then the presence of the strength of nonlinearity of the electromagnetic field decreases the magnitudes of oscillation in the Hayward–class.

In the Fig 3 d) we show and compare the real part of the quasi–normal frequencies for

$n$	$l$	New-class			Bardeen-class			Hayward-class			
		$q$	$\omega_{r_{sc}}$	$\omega_{r_{elec}}$	$q$	$\omega_{r_{sc}}$	$\omega_{r_{elec}}$	$q$	$\omega_{r_{sc}}$	$\omega_{r_{elec}}$	
0	2	0.04	0.268903	0.241723	0.10	0.225775	0.201529	0.01	0.224122	0.199931	
		0.08	0.338162	0.307184	0.28	0.238258	0.213655	0.51	0.22413	0.199942	
		0.12	0.468511	0.433139	0.46	0.271251	0.24633	1.01	0.224577	0.200559	
	3	0.04	0.534147	0.506741	0.10	0.44974	0.425251	0.01	0.446589	0.422154	
		0.08	0.669362	0.638181	0.28	0.473542	0.448699	0.51	0.446608	0.422175	
		0.12	0.923967	0.888386	0.46	0.536847	0.511641	1.01	0.447752	0.423441	
	4	0.04	0.887601	0.860099	0.10	0.748136	0.723546	0.01	0.742986	0.71845	
		0.08	1.11078	1.07951	0.28	0.787037	0.762091	0.51	0.743021	0.718486	
		0.12	1.53105	1.49538	0.46	0.89072	0.86539	1.01	0.745048	0.720616	
	1	3	0.04	0.435158	0.408867	0.10	0.354413	0.331169	0.01	0.350682	0.327503
			0.08	0.569975	0.539723	0.28	0.382793	0.359134	0.51	0.350715	0.327542
			0.12	0.834249	0.799553	0.46	0.458791	0.434885	1.01	0.352538	0.329684
4		0.04	0.789045	0.76225	0.10	0.653297	0.629464	0.01	0.647573	0.6238	
		0.08	1.01175	0.981052	0.28	0.696747	0.672526	0.51	0.647622	0.623853	
		0.12	1.44168	1.40655	0.46	0.813163	0.788633	1.01	0.650407	0.62686	
5		0.04	1.23101	1.20392	0.10	1.02647	1.00233	0.01	1.01825	0.99417	
		0.08	1.56364	1.53271	0.28	1.08878	1.06427	0.51	1.01831	0.994241	
		0.12	2.20065	2.16529	0.46	1.25567	1.23082	1.01	1.02223	0.998329	
2		4	0.04	0.566146	0.540069	0.10	0.434374	0.41139	0.01	0.42654	0.403617
			0.08	0.79612	0.766077	0.28	0.494176	0.470837	0.51	0.426711	0.403799
			0.12	1.26079	1.22661	0.46	0.653567	0.630448	1.01	0.436477	0.414207
	5	0.04	1.00836	0.981766	0.10	0.807822	0.784259	0.01	0.797492	0.773987	
		0.08	1.34822	1.31774	0.28	0.886491	0.862578	0.51	0.797685	0.774188	
		0.12	2.02007	1.98536	0.46	1.09653	1.07263	1.01	0.808718	0.785677	
	6	0.04	1.53869	1.5118	0.10	1.2556	1.2317	0.01	1.24227	1.21843	
		0.08	2.01048	1.97973	0.28	1.35691	1.33267	0.51	1.24249	1.21865	
		0.12	2.93087	2.89585	0.46	1.62761	1.60326	1.01	1.25493	1.23144	

TABLE III: Third-order WKB approximation of  $\omega_r$  with different values of  $n$  and  $l$ . The mass is fixed to  $M = 1$  and  $\mu = 6$

the three classes of BHs, in the case  $\mu = 6$ , in general  $\omega_{r_{(New-class)}} > \omega_{r_{(Bardeen-class)}} > \omega_{r_{(Hayward-class)}}$  for both perturbations. Then the electromagnetic perturbations present slower oscillations than the scalar ones, the Hayward-class has the slowest oscillations.

The complex quasinormal frequencies are shown in Fig. 4. In the case of the New-class (see Fig. 4 a) )  $|\omega_i|$  increase with increasing values of  $q$  for the scalar and electromagnetic perturbations and  $|\omega_{i_{sc}}| > |\omega_{i_{elec}}|$ . If  $\mu$  increases,  $\omega_i$  increases but the range of values for  $q$  decreases.

Now in the case of the Bardeen-class and Hayward-class, in the Fig 4 a), b) we can observe that the imaginary part of QNM frequencies  $|\omega_i|$ , increases as  $q$  augments and shows a maximum, then it decreases, the value of  $q$  cannot exceed  $q_{crit}$ , which corresponds to the extreme BH. Also in the Bardeen-class and Hayward-class  $|\omega_{i_{sc}}| > |\omega_{i_{elec}}|$ .

If we make the comparison of  $\omega_i$  of the different BHs (see Fig 4 d)) for a fixed  $\mu = 6$ , we observe that in a certain range  $|\omega_{i_{(New-class)}}| > |\omega_{i_{(Bardeen-class)}}| > |\omega_{i_{(Hayward-class)}}|$ .

One of the important properties of the perturbations is the relaxation time, which is

$n$	$l$	New-class			Bardeen-class			Hayward-class		
		$q$	$ \omega_{i_{sc}} $	$ \omega_{i_{elcc}} $	$q$	$ \omega_{i_{sc}} $	$ \omega_{i_{elcc}} $	$q$	$ \omega_{i_{sc}} $	$ \omega_{i_{elcc}} $
0	2	0.04	0.107577	0.1008	0.10	0.0966757	0.0901323	0.01	0.0966011	0.090031
		0.08	0.121123	0.114282	0.28	0.0969466	0.090609	0.51	0.0965849	0.0900147
		0.12	0.134579	0.12814	0.46	0.0946585	0.0888299	1.01	0.0955937	0.089004
	3	0.04	0.147717	0.142867	0.10	0.132426	0.127751	0.01	0.132302	0.127609
		0.08	0.166856	0.161952	0.28	0.132952	0.123414	0.51	0.13228	0.127587
		0.12	0.186146	0.181533	0.46	0.130067	0.125876	1.01	0.130896	0.126183
	4	0.04	0.188437	0.184661	0.10	0.168763	0.165126	0.01	0.168594	0.164944
		0.08	0.213134	0.209314	0.28	0.169508	0.165974	0.51	0.168565	0.164915
		0.12	0.238173	0.234579	0.46	0.165952	0.162682	1.01	0.166788	0.163121
1	3	0.04	0.441892	0.427338	0.10	0.306012	0.381987	0.01	0.395615	0.381536
		0.08	0.499447	0.484731	0.28	0.397756	0.384146	0.51	0.395544	0.381466
		0.12	0.55741	0.543582	0.46	0.389208	0.376662	1.01	0.391203	0.377084
	4	0.04	0.56405	0.552721	0.10	0.505022	0.494111	0.01	0.504491	0.49354
		0.08	0.638278	0.626815	0.28	0.507424	0.496825	0.51	0.504401	0.49345
		0.12	0.713496	0.702722	0.46	0.496872	0.487081	1.01	0.498889	0.487899
	5	0.04	0.687012	0.677737	0.10	0.614837	0.605908	0.01	0.614178	0.605217
		0.08	0.777871	0.768484	0.28	0.617854	0.609176	0.51	0.614069	0.605108
		0.12	0.87022	0.861396	0.46	0.605204	0.597177	1.01	0.607386	0.598389
2	4	0.04	0.935883	0.916994	0.10	0.837481	0.819299	0.01	0.836511	0.818263
		0.08	1.06006	1.04094	0.28	0.842041	0.824387	0.51	0.836353	0.818104
		0.12	1.18575	1.16782	0.46	0.824842	0.808581	1.01	0.826562	0.808281
	5	0.04	1.14082	1.12535	0.10	1.02051	1.00563	0.01	1.01932	1.00439
		0.08	1.29271	1.27706	0.28	1.02609	1.01164	0.51	1.01913	1.0042
		0.12	1.44696	1.43228	0.46	1.00541	0.992074	1.01	1.0074	0.992432
	6	0.04	1.34648	1.33339	0.10	1.20426	1.19166	0.01	1.20286	1.19023
		0.08	1.52605	1.5128	0.28	1.21083	1.1986	0.51	1.20264	1.19001
		0.12	1.70876	1.69632	0.46	1.18659	1.17528	1.01	1.18897	1.17629

TABLE IV: Third-order WKB approximation of  $\omega_i$  with different values of  $n$  and  $l$ . The mass is fixed to  $M = 1$  and  $\mu = 6$

defined by the inverse of the imaginary part of QNM ( $\tau = 1/|\omega_i|$ ). It is clear that the relaxation time of the New-class diminishes faster compared with the Bardeen-class and Hayward-class (see Fig 4 d)), implying that the New-class system recovers the stationary state faster for both perturbations. Comparing the relaxation times for the scalar and electromagnetic perturbations  $\tau_{(New-class)} < \tau_{(Bardeen-class)} < \tau_{(Hayward-class)}$  for charges  $q < 0.12$ . However, when  $q$  approaches its upper bound ( $q_{crit}$ ) the relaxation time grows, giving then a longer life to perturbations in the cases of Bardeen-class and Hayward-class.

## V. GREYBODY FACTOR

This section will discuss the reflection and transmission coefficients for scalar and electromagnetic perturbations of the different classes of black holes.

In the case of considering an incoming wave towards an black hole, the wave is partially transmitted and partially reflected by the potential barrier (16). This case is different from

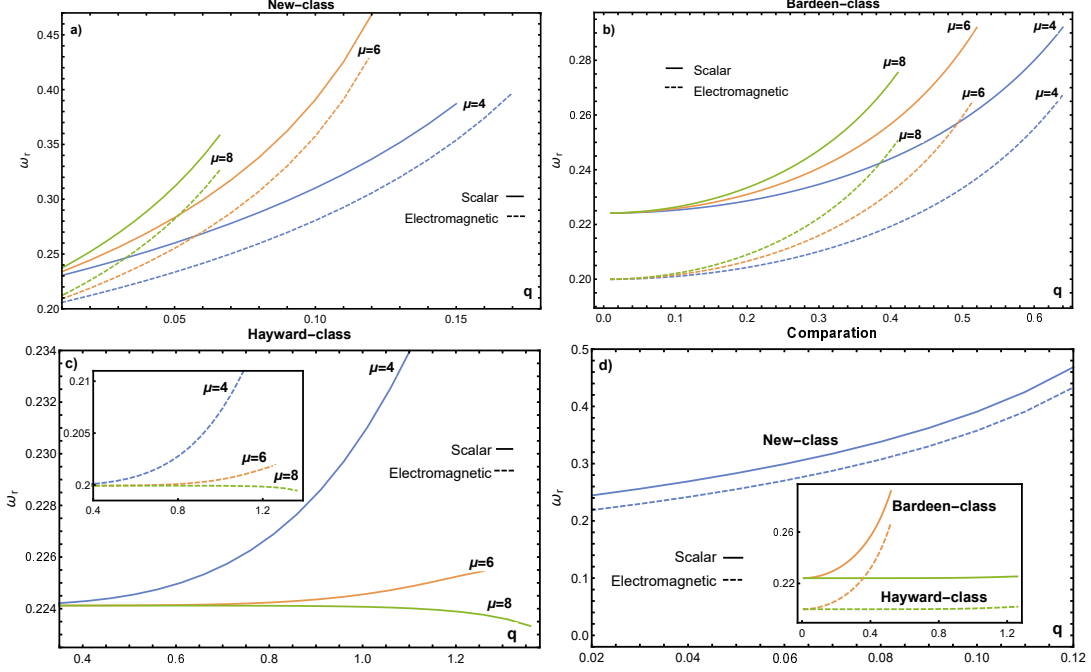


FIG. 3: The behavior of  $\omega_r$  in the fundamental mode  $n = 0$  for the different BHs are shown as a function of  $q$  and  $l = 2$ . In all the figures, the scalar perturbation is denoted with a solid line and electromagnetic perturbation is denoted with a dashed line. a) Shows the behavior of  $\omega_r$  for the New-class with  $M = 1$  and  $\mu = 4, 6, 8$ . b) Shows the behavior of  $\omega_r$  for the Bardeen-class with  $M = 1$  and  $\mu = 4, 6, 8$ . c) Shows the behavior of  $\omega_r$  for the Hayward-class with  $M = 1$  and  $\mu = 4, 6, 8$ . d) The behaviors of  $\omega_r$  are compared for the different BHs with  $\mu = 6$  and  $M = 1$ .

the quasinormal frequencies calculation since we relax the boundary condition of incoming waves from infinity. So, the scattering behavior of the wave (with a frequency  $\omega$ ) can be written in tortoise coordinates as;

$$\xi(r_*) = T(\omega)e^{-i\omega r_*}, \quad r_* \rightarrow -\infty, \quad (21)$$

$$\xi(r_*) = e^{-i\omega r_*} + R(\omega)e^{i\omega r_*}, \quad r_* \rightarrow \infty, \quad (22)$$

where  $R(\omega)$  and  $T(\omega)$  are the reflection and transmission coefficients, respectively. Let us note, that the wave frequency  $\omega$  is real. The relation between the reflection and transmission coefficients from the flux conservation is given by;

$$|R(\omega)|^2 + |T(\omega)|^2 = 1. \quad (23)$$

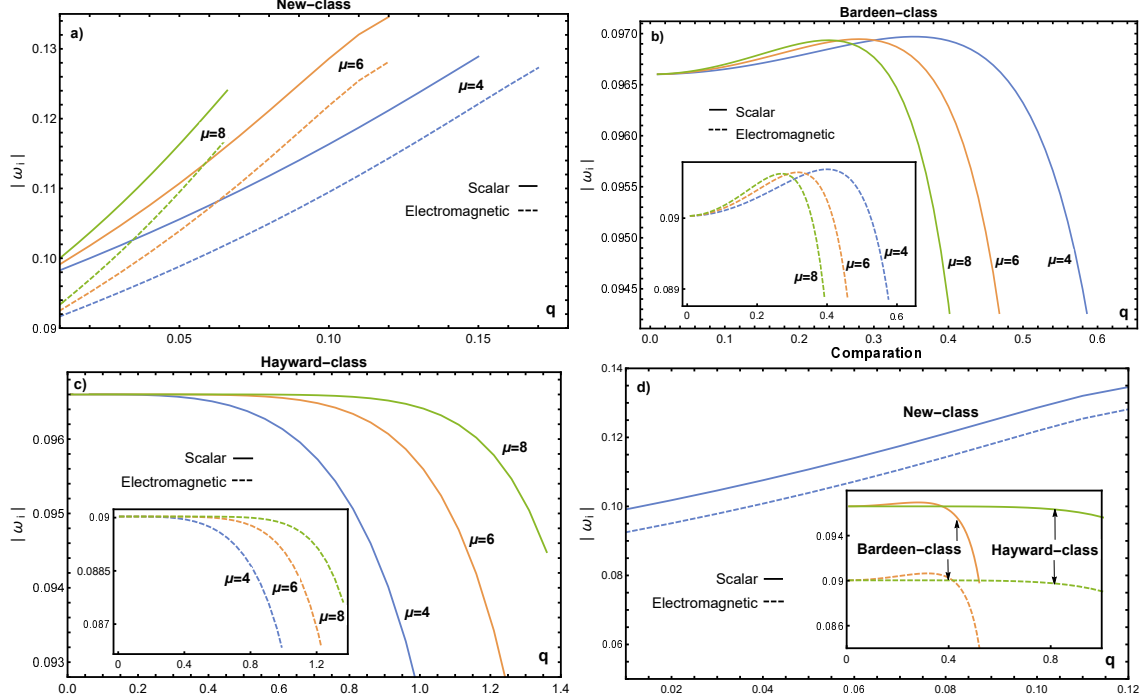


FIG. 4: The behavior of  $|\omega_i|$  in the fundamental mode  $n = 0$  for the different BHs is shown as a function of  $q$  and  $l = 2$ . In all the figures, the scalar perturbation is denoted with a solid line and electromagnetic perturbation is denoted with a dashed line. a) Shows the behavior of  $|\omega_i|$  for the New-class with  $M = 1$  and  $\mu = 4, 6, 8$ . b) Shows the behavior of  $|\omega_i|$  for the Bardeen-class with  $M = 1$  and  $\mu = 4, 6, 8$ . c) Shows the behavior of  $\omega_i$  for the Hayward-class with  $M = 1$  and  $\mu = 4, 6, 8$ . d) The behaviors of  $|\omega_i|$  are compared for the different BHs with  $\mu = 6$  and  $M = 1$ .

If the incoming wave has a smaller frequency than the height of the potential barrier ( $\omega^2 \ll V_0$ ), then the transmission coefficient is close to zero, and the reflection coefficient is close to one. On the other hand, if  $\omega^2 \gg V_0$ , then the reflection coefficient is close to zero, while the transmission coefficient is close to one, in other words, the wave will not be reflected by the barrier of potential.

However, if  $\omega^2 \approx V_0$  the WKB approximation has high accuracy, Then in this case, the greybody factor can be calculated. Greybody factor is understood as the probability for an outgoing wave with a  $\omega$  to reach infinity or, equivalently, the absorption probability for an incoming wave with a  $\omega$  to be absorbed by the black hole.

Then in the WKB approximation and  $\omega^2 \approx V_0$ , the reflection coefficient is given by;

$$R(\omega) = (1 + e^{-2\pi i\beta})^{-1/2}, \quad (24)$$

where to third-order in the WKB approximation,  $\beta$  can be determined from the following equation;

$$\beta - i \frac{\omega^2 - V_0}{\sqrt{-2V_0''}} + \Lambda(\beta) - \beta\Omega(\beta) = 0, \quad (25)$$

where  $\Lambda(\beta)$  and  $\Omega(\beta)$  are given by Eqs. (18) and (19), respectively. From Eq. (24) we can express the greybody factor as;

$$\gamma_l(\omega) = |T(\omega)|^2 = 1 - \left| (1 + e^{-2\pi i\beta})^{-1/2} \right|^2. \quad (26)$$

Using the solutions (21) and (22), the absorption cross-section of planar massless scalar waves can be written as  $\sigma_{abs} = \sum_{l=0}^{\infty} \sigma_l(\omega)$ , where the partial absorption cross-section ( $\sigma_l(\omega)$ ) of the wave for a given frequency  $\omega$  and  $l$  is given by;

$$\sigma_l(\omega) = \frac{\pi(2l+1)}{\omega^2} \gamma_l(\omega). \quad (27)$$

The numerical results of the reflection and transmission coefficients for the different black holes classes (New-class, Bardeen-class and New-class) in terms of different values of parameter  $\mu$  are shown in Figs. 5–7. Fig. 5 a) shows how the reflection coefficient increases with an increasing  $\mu$  with the New-class and the Fig. 5 b) shows the opposite behavior for the transmission coefficient. However, in the case of the scalar perturbation the effect is more noticeable than in the case of the electromagnetic perturbation for the reflection coefficient.

Fig. 6 a) and b) shows the reflection coefficient and the transmission coefficient of the Bardeen-class for different  $\mu$ , the differences between the coefficients  $|R(\omega)|^2$  or  $|T(\omega)|^2$  for different  $\mu$ , are more close for both perturbations. And as in the New-class electromagnetic perturbation, the effect is more noticeable than in the case of the scalar perturbation for the transmission coefficient.

The reflection and transmission coefficients of Hayward-class are shown as a function of  $\omega$  with different values of  $\mu$  in Figs. 7 a) and b). The reflection coefficient is very close in the cases  $\mu = 6$  and  $\mu = 8$ . The same happens in the case of the transmission coefficient (it is observed for both perturbations). In the small box, the difference is shown.



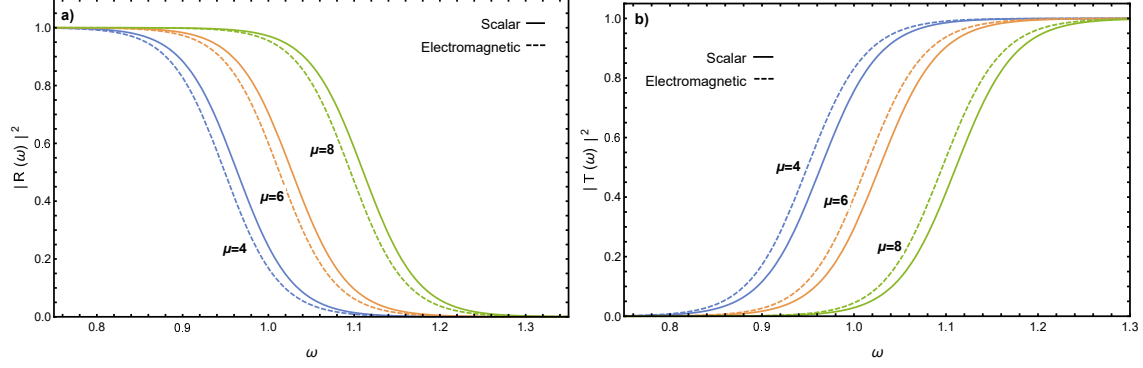


FIG. 5: The reflection and transmission coefficients for the New-class are shown as a function of  $\omega$  with different values of  $\mu$ ,  $M = 1$ ,  $q = 0.07$  and  $l = 4$ . a) Shows the behavior of  $|R(\omega)|^2$ . b) Shows the behavior of  $|T(\omega)|^2$ .

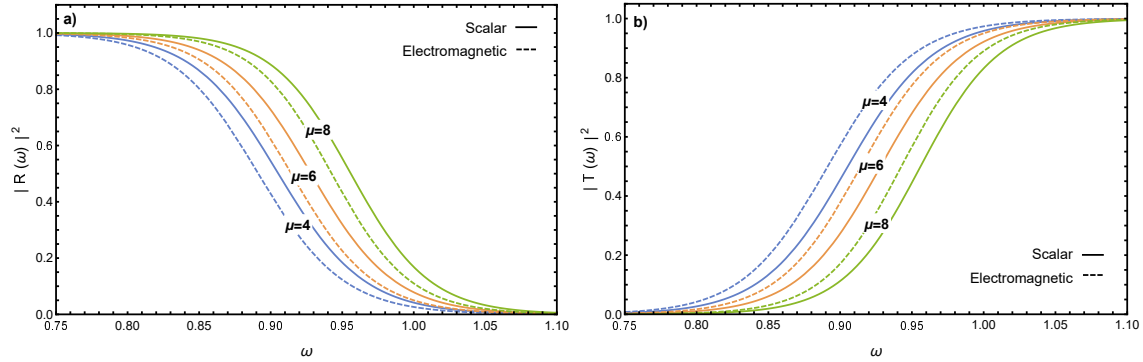


FIG. 6: The reflection and transmission coefficients for the Bardeen-class are shown as a function of  $\omega$  with different values of  $\mu$ ,  $M = 1$ ,  $q = 0.41$  and  $l = 4$ . a) Shows the behavior of  $|R(\omega)|^2$ . b) Shows the behavior of  $|T(\omega)|^2$ .

It is clear that the effect of  $\mu$  is to diminish the transmission coefficient for the New-class and Bardeen-class, but in Hayward-class it increases. Implying then that when the strength of nonlinearity of the electromagnetic field increases the transmission of the wave decreases, for any of the perturbations in New-class and Bardeen-class. And, an increase in the strength of nonlinearity of the electromagnetic field increases the transmission for Hayward-class. In general we can mention that  $|R(\omega)|^2_{New-class} > |R(\omega)|^2_{Bardeen-class} > |R(\omega)|^2_{Hayward-class}$  and  $|T(\omega)|^2_{Hayward-class} > |T(\omega)|^2_{Bardeen-class} > |T(\omega)|^2_{New-class}$ , when the  $\mu$  parameter is fixed and we have the same values of  $q$ ,  $M$  and  $l$ .

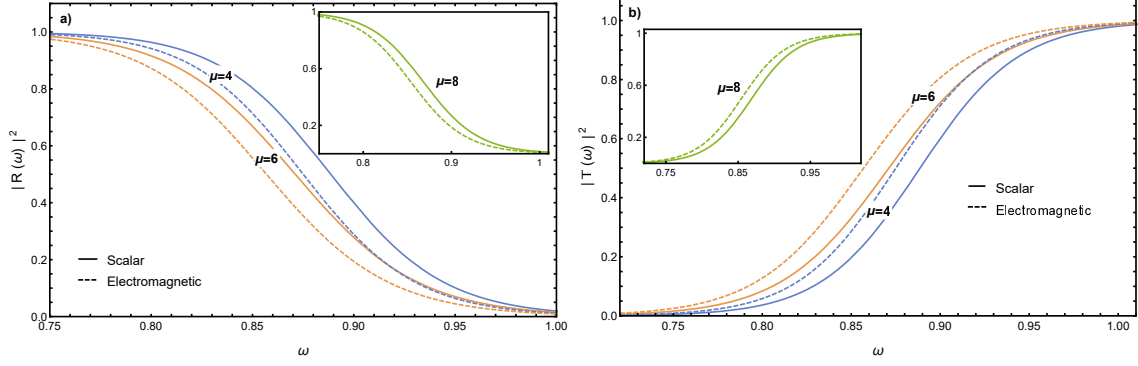


FIG. 7: The reflection and transmission coefficients for the Hayward-class are shown as a function of  $\omega$  with different values of  $\mu$ ,  $M = 1$ ,  $q = 1.13$  and  $l = 4$ . a) Shows the behavior of  $|R(\omega)|^2$ . b) Shows the behavior of  $|T(\omega)|^2$ .

The partial absorption cross-section is higher for Hayward-class and Bardeen-class as shown in Fig. 8 a) and b). This is expected since the heights of the effective potentials in Fig. 2 d) for Hayward-class and Bardeen-class are less than the effective potential of New-class. Thus, there is less absorption for the New-class. On the other hand, by comparing the absorption cross-section to those related to scalar and electromagnetic fields, we can conclude that  $\sigma_{l(elec)} > \sigma_{l(sc)}$ . We can mention that the absorption cross-section Hayward-class is very close to the absorption cross-section Bardeen-class.

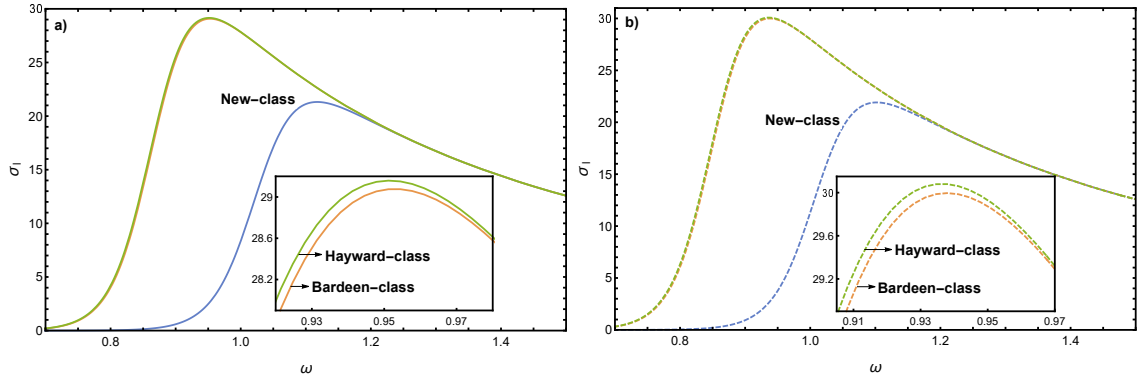


FIG. 8: The different  $\sigma_l$  are shown for  $l = 4$ ,  $\mu = 6$ ,  $q = 0.07$  and  $M = 1$ . a) The different  $\sigma_l$  are shown for scattered scalar. b) The different  $\sigma_l$  are shown for scattered electromagnetic

## VI. CONCLUSIONS

We analyzed a Generic-class of magnetically charged regular black hole that contain the Bardeen-class, Hayward-class, and a New-class solutions, we have expressed the radial distance and the parameter of charge in units of mass for the analysis of horizons and the extreme case, we presented how  $q$  depends on the values of  $\mu$ . Also, the critical mass is obtained.

Then, analyzing the effective potential of scalar and electromagnetic perturbations, we have shown that the effective potentials of scalar perturbations are larger compared to the effective potentials of the electromagnetic perturbations in all cases. It is also possible to mention that  $V(r)_{Hayward-class} < V(r)_{Bardeen-class} < V(r)_{New-class}$  when we fix  $\mu$ . When  $\mu$  is increased, the maximum potentials increase for New-class and Bardeen-class, but for Hayward-class it is opposite.

We studied the QNM of the scalar and electromagnetic perturbations in the Generic-class of magnetically charged regular black holes using the third-order WKB method. Results have shown that an increase in  $q$  implies a monotonic increase of the real part of the QNM frequency of New-class and Bardeen-class. On the other hand, we can see that with an increase in the parameter  $\mu$ , the real part of the QNM frequencies increases. But in the case of Hayward-class when we increase the parameter  $\mu$ , the real part of the QNM frequencies decreases.

We find that in the Generic-class, the imaginary part of the QNM is always larger for the scalar perturbation and smaller for electromagnetic perturbation. However, the roles are swapped for the relaxation time, we also observe that in a certain range  $|\omega_{i(New-class)}| > |\omega_{i(Bardeen-class)}| > |\omega_{i(Hayward-class)}|$ .

It is possible to set as the presence of strength of nonlinearity of the electromagnetic field increases or decreases the magnitudes of oscillation and relaxation times of the different kinds of solutions. Being the New-class, the most stable solution for scalar and electromagnetic perturbation, but the range of the values of  $q$  is small.

The greybody factor has been calculated by applying the third-order WKB approach for the two different types of perturbations. The greybody factor decreases with an increasing of  $\mu$  to the New-class and Bardeen-class while for the Hayward-class increases with an increase in  $\mu$ , i.e., the probability of the wave transmission through the potential barrier depends

inversely on the maximum of the effective potential, and this behavior can be explained from the Fig. 2 d).

Thus, in the Hayward–class, an increase in the value of the  $\mu$  weakens the potential barrier in relation, and hence the transmission coefficient increases. And said behavior behaves oppositely in the cases of New–class and Bardeen–class.

## ACKNOWLEDGMENT

L. A. López acknowledge the partial financial support of SNI–CONACYT, México.

- 
- [1] M. Born and L. Infeld. Foundations of the new field theory. *Proc. Roy. Soc. Lond. A*, 144(852):425–451, 1934.
  - [2] Eloy Ayon-Beato and Alberto Garcia. The Bardeen model as a nonlinear magnetic monopole. *Phys. Lett. B*, 493:149–152, 2000.
  - [3] Joseph Polchinski. Decoupling Versus Excluded Volume or Return of the Giant Wormholes. *Nucl. Phys.*, B325:619–630, 1989.
  - [4] Sean A. Hayward. Formation and evaporation of regular black holes. *Phys. Rev. Lett.*, 96:031103, 2006.
  - [5] Zhong-Ying Fan and Xiaobao Wang. Construction of regular black holes in general relativity. *Phys. Rev. D*, 94:124027, Dec 2016.
  - [6] B. P. Abbott et al. GW151226: Observation of Gravitational Waves from a 22-Solar-Mass Binary Black Hole Coalescence. *Phys. Rev. Lett.*, 116(24):241103, 2016.
  - [7] Jake Percival and Sam R. Dolan. Quasinormal modes of massive vector fields on the Kerr spacetime. *Phys. Rev. D*, 102(10):104055, 2020.
  - [8] Hong Ma and Jin Li. Dirac quasinormal modes of Born-Infeld black hole spacetimes. *Chin. Phys. C*, 44(9):095102, 2020.
  - [9] Bernard F. Schutz and Clifford M. Will. BLACK HOLE NORMAL MODES: A SEMIANALYTIC APPROACH. *Astrophys. J. Lett.*, 291:L33–L36, 1985.
  - [10] Sharmanthie Fernando and Juan Correa. Quasinormal modes of the bardeen black hole: Scalar perturbations. *Phys. Rev. D*, 86:064039, Sep 2012.

- [11] Sharmanthie Fernando. Gravitational perturbation and quasi-normal modes of charged black holes in Einstein-Born-Infeld gravity. *Gen. Rel. Grav.*, 37:585–604, 2005.
- [12] Jin Li, Kai Lin, and Nan Yang. Nonlinear electromagnetic quasinormal modes and Hawking radiation of a regular black hole with magnetic charge. *Eur. Phys. J. C*, 75(3):131, 2015.
- [13] Bobir Toshmatov, Zdeněk Stuchlík, and Bobomurat Ahmedov. Electromagnetic perturbations of black holes in general relativity coupled to nonlinear electrodynamics: Polar perturbations. *Phys. Rev. D*, 98(8):085021, 2018.
- [14] Bobir Toshmatov, Zdeněk Stuchlík, Jan Schee, and Bobomurat Ahmedov. Electromagnetic perturbations of black holes in general relativity coupled to nonlinear electrodynamics. *Phys. Rev. D*, 97(8):084058, 2018.
- [15] Bobir Toshmatov, Ahmadjon Abdujabbarov, Zdeněk Stuchlík, and Bobomurat Ahmedov. Quasinormal modes of test fields around regular black holes. *Phys. Rev. D*, 91(8):083008, 2015.
- [16] N. Breton and L. A. Lopez. Quasinormal modes of nonlinear electromagnetic black holes from unstable null geodesics. *Phys. Rev. D*, 94(10):104008, 2016.
- [17] Nora Breton and L. A. López. Birefringence and quasinormal modes of the einstein-euler-heisenberg black hole. *Phys. Rev. D*, 104:024064, Jul 2021.
- [18] M. Novello, V. A. De Lorenci, J. M. Salim, and R. Klippert. Geometrical aspects of light propagation in nonlinear electrodynamics. *Phys. Rev. D*, 61:045001, Jan 2000.
- [19] Kirill A. Bronnikov. Comment on “construction of regular black holes in general relativity”. *Phys. Rev. D*, 96:128501, Dec 2017.
- [20] Bobir Toshmatov, Zdeněk Stuchlík, and Bobomurat Ahmedov. Comment on “construction of regular black holes in general relativity”. *Phys. Rev. D*, 98:028501, Jul 2018.
- [21] Bobir Toshmatov, Zdeněk Stuchlík, and Bobomurat Ahmedov. Rotating black hole solutions with quintessential energy. *Eur. Phys. J. Plus*, 132(2):98, 2017.
- [22] Muhammad Rizwan, Mubasher Jamil, and Anzhong Wang. Distinguishing a rotating kiselev black hole from a naked singularity using the spin precession of a test gyroscope. *Phys. Rev. D*, 98:024015, Jul 2018.
- [23] Bobir Toshmatov, Zdeněk Stuchlík, Bobomurat Ahmedov, and Daniele Malafarina. Relaxations of perturbations of spacetimes in general relativity coupled to nonlinear electrodynamics. *Phys. Rev. D*, 99:064043, Mar 2019.

- [24] A. J. M. Medved, Damien Martin, and Matt Visser. Dirty black holes: Symmetries at stationary nonstatic horizons. *Phys. Rev. D*, 70:024009, 2004.
- [25] Hidefumi Nomura and Takashi Tamaki. Continuous area spectrum of a regular black hole. *Phys. Rev. D*, 71:124033, Jun 2005.
- [26] R. A. Konoplya, A. Zhidenko, and A. F. Zinhailo. Higher order WKB formula for quasinormal modes and grey-body factors: recipes for quick and accurate calculations. *Class. Quant. Grav.*, 36:155002, 2019.
- [27] Sai Iyer and Clifford M. Will. Black Hole Normal Modes: A WKB Approach. 1. Foundations and Application of a Higher Order WKB Analysis of Potential Barrier Scattering. *Phys. Rev. D*, 35:3621, 1987.
- [28] R. A. Konoplya. Quasinormal behavior of the d-dimensional Schwarzschild black hole and higher order WKB approach. *Phys. Rev. D*, 68:024018, 2003.